

Study on a falling metal drop in a perpendicular magnetic field

F. Garzón

Instituto de Investigación en Ciencias Básicas y Aplicadas, Universidad Autónoma del Estado de Morelos, México.

G. Ramírez

*Instituto de Energías Renovables, Universidad Autónoma del México,
Temixco, Morelos, 62580 México.*

S. Piedra

*CONACYT-CIDESI, Centro Nacional de Tecnologías Aeronáuticas,
Querétaro, Qro., 76270, México.*

A Figueroa

*CONACYT-Centro de Investigación en Ciencias, Universidad Autónoma del Estado de Morelos, México.
e-mail: alfil@uaem.mx*

Received 24 June 2021; accepted 29 October 2021

A theoretical and experimental study of a falling metal drop which interacts with a perpendicular non-localized magnetic field is addressed. As the metal drops traverses the magnetic field, it suffers a braking due to induced electromagnetic effects. An analytical solution for the velocity of the falling drop is obtained through a balance of forces which affect its motion. A numerical solution from the incompressible Navier-Stokes equations for two phase flows is also obtained. A numerical model for the solution of the incompressible Navier-Stokes for two-phase flows is also implemented. This model is based in the front-tracking/finite volume method. The simulation allows observe a more detailed dynamics such as the deformation of the drop. Both the theoretical and numerical results validate the experimental data obtained through the Particle Image Velocimetry.

Keywords: Navier-Stokes equations; particle image velocimetry.

DOI: <https://doi.org/10.31349/RevMexFis.68.030601>

1. Introduction

Magnetohydrodynamics (MHD) is concerned with the interaction of flowing fluids and magnetic fields. The fluid in question must be electrically conducting and non-ferromagnetic such as metal-based fluids, plasmas and electrolytes [1]. Theoretical models of MHD flows are formulated by coupling the Navier-Stokes equations and Maxwell's equations, both systems of equations couple via the Lorentz force. Numerous studies have already been conducted on MHD flows for industrial applications such as heat sinks in nuclear reactors, pumps, batteries and levitating liquid metals.

On the interaction between liquid metal and magnetic fields, numerous experimental investigations of metal fluids flowing through a channel to which an artificial external magnetic field is applied have been performed [2–4]. A fluid electrically conducting that flows through a channel in the presence of an external magnetic field produced by a magnet suffers a magnetic braking in its momentum by Lorentz force, *i.e.*, induced electric currents are produced inside the entire fluid flow due the relative movement to the applied magnetic field, thus the Lorentz force results in an induced magnetic force in the opposite direction of fluid flow, thereby causing the fluid to slow its motion. This effect has also been observed experimentally in the case of a rising single helium bubble in

a metal liquid environment like mercury under vertical magnetic field [5], which demonstrate that the rise velocity of helium bubble decreases monotonically with the increase of the magnetic field. The latter results were confirmed with numerical simulations by means of two-phase interface treatment [6, 7].

In particular, the dynamics of liquid metal jets/drops is important, for example, in the development of alternative energy sources such as new plasma-based fusion reactors like the Tokamak [8], or the development of revolutionary three-dimensional printing based on liquid metal generated by melting which is printed using an ink-jetting process [9]. Furthermore, studies of exoplanet atmospheres such as those of the giant exoplanet WASP-76b [10] demonstrate the possibility of molten iron raining as droplets. It is suspected that this rainfall is affected by induced MHD effects.

The effect on the motion of a liquid metal drop falling in presence of a magnetic field was studied first by [11]. The authors computed the force promoted by the interaction of the induced electric currents generated into the drop and the applied magnetic field. They concluded that no matter the sign of the magnetic field gradient, the electromagnetic force is always in the opposite direction of the drop motion, acting as an electromagnetic drag. More recently, the study of a falling metal drop was performed by a numerical simulation [12], where a drop fell into a metal liquid layer in the

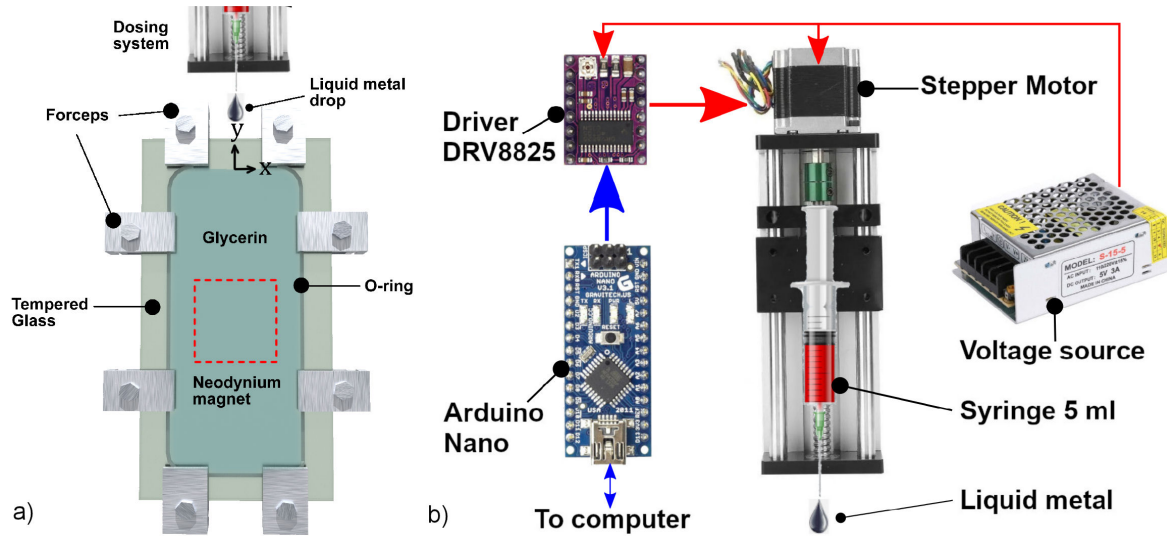


FIGURE 1. Sketch of the experimental set-up, not drawn to scale. a) Hele-Shaw cell. The flow promoted by falling drop is visualized in the x - y plane through the PIV technique. b) Diagram of the liquid metal droplet dosing system and its components. Blue lines indicate the flow of control signals and red lines indicate the flow of electrical current.

presence of imposed vertical magnetic field, such results revealed an interesting behaviour on metal liquid layer for a strong magnetic field, spreading was substantially reduced and a swelling of free surface after collision were observed. An interesting investigation is presented in Ref. [13], where numerical simulations were performed of a falling droplet in the presence of a positive and negative magnetic field gradient.

In contrast to previous works, we present a theoretical and experimental study of a falling metal drop under the effect of a perpendicular magnetic field. The experimental set-up is rather simple and useful which does not require expensive high speed cameras since it is a liquid-liquid phase experiment. Additionally, in the numerical simulations a real distribution of the magnetic field was used in order to compare the phenomenon with the experimental observations.

2. Experimental procedure

The experiment set up consist of a liquid metal drop falling in a Hele-Shaw cell. The cell consist of two sheets of tempered glass glued to an O-ring and kept fixed with aluminium forceps. The cell's dimensions are 230 mm long 110 mm width and a separation between sheets of 2.5 mm. The cell is vertically placed and is open in the upper side, see Fig. 1. A rectangular parallelepiped Neodymium magnet with a side length of 50.8 mm, height of 25.4 mm is placed in the geometrical center outside the cell. The z -axis of the magnet is perpendicular to the cell. The perpendicular component of the magnetic field was measured with a Teslameter F.W. BELL, model 4048. The maximum strength of the magnetic field at the cell's centre is 0.22 T, as seen in Fig. 2.

The formation of liquid metal drops was carried out by automating a 5 ml syringe. It was manually filled with liq-

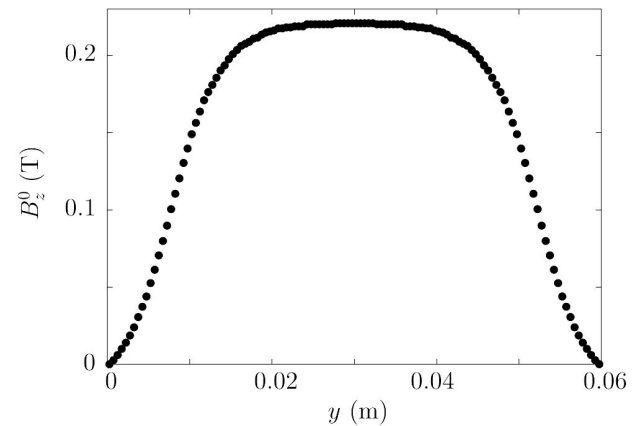


FIGURE 2. Perpendicular component B_z^0 of the magnetic field as a function of the y -coordinate in the PIV observation zone. Dots denote experimental measurements.

uid metal during testing, later it is placed on a screw linear actuator (six centimeters of travel), the which implements a stepper motor (nema 17) to linearly move the plunger of the syringe. The volume of the drop ($V = 0.022$ ml) is controlled by varying the angular velocity and the number of steps of the motor, for this purpose, an Arduino Nano microcontroller and the DRV8825 driver are used. The latter generated liquid metal drops with diameter $d = 3.4$ mm. Figure 1b) shows the components used for dosing drops of liquid metal. The measures of the cell were calculated so that its boundaries are sufficiently far away from the metal drop.

In order to obtain low Reynolds flows, the cell was filled with glycerin rather than air, thus the drag is increased. The working fluids are at room temperature (20° C). The drop is an eutectic alloy of Gallium, Indium and Tin (GaInSn) that is liquid at room temperature; its mass density, kinematic

viscosity and electrical conductivity are $\rho_1 = 6360 \text{ Kg/m}^3$, $\nu = 3.4 \times 10^{-7} \text{ m}^2/\text{s}$ and $\sigma = 3.46 \times 10^6 \text{ S/m}$, respectively. The glycerin ($\rho_2 = 1261 \text{ Kg/m}^3$) is seeded with hollow glass spheres, with an approximated diameter of $10 \mu\text{m}$. The high surface tension between glycerin and the liquid metal ($537 \pm 13 \text{ mN/m}$ [14]) promotes that the flow is dominated by the surface tension force and the drops take an approximately a circular and / or elliptical shape within the Hele Shaw cell. Since the drop reaches small velocities because of the drag with the glycerin, images of the falling metal drop were recorded with a common photographic camera rather than a high speed camera. We used a Nikon D90 with a AF micro-nikkor 60mm f/2.8D lens. For the tracking of the drop, an image analysis algorithm was used to detect the pixels that correspond to the boundary of the drop in the plane of the cell (Circular Hough algorithm). The Particle Image Velocimetry (PIV) technique was used in order to obtain velocity vector fields. The actual area of the captured image was $0.03 \text{ m} \times 0.06 \text{ m}$ in the central part of the cell, where the drop has reached a terminal velocity. The images had 1280×720 pixels resolution. Avoiding the transient flow, we obtained 24 snapshots per second. The PIVlab software was used to perform the analysis [15]; we used interrogation areas of 32×32 pixels with 50% overlap in the horizontal and vertical directions, and vector validation. The error in the experimental data was obtained by adjusting a normal distribution to the data at sample points. The relative error is smaller than 18%.

3. Theoretical model

3.1. Numerical solution

Consider a two dimensional fluid composed by two-immiscible fluids (a continuous phase and a liquid metal droplet) in presence of the acceleration of gravity. The distribution of the magnetic field is modeled as in Ref. [16] that corresponds to the distribution found experimentally, as seen in Fig. 2. The drop falls due to its weight and the continuous phase is displaced by the moving drop. The surface tension between the two fluids is taken into account in the model, and the geometry of the interface is calculated by considering the normal and tangential stresses that arise due to the interaction of the drops and the surrounding liquid. Due to the complexity of the problem, it was approached numerically by a finite volume/front-tracking method where a single set of conservation equations [17] are solved for the entire domain, including the liquid metal drop and the continuous phase. The details of the numerical implementation can be found in Ref. [18]. The equations that describe the motion of the drops and the surrounding are mass and momentum conservation coupled with electromagnetic equations for computing the induced magnetic field with the low magnetic Reynolds number approximation [1, 19]. Considering that the two fluids are incompressible, the mass conservation is given by:

$$\nabla \cdot \mathbf{u} = 0, \quad (1)$$

where \mathbf{u} is the fluid velocity. The momentum conservation equation is written in a form that includes the different fluids and the surface tension force:

$$\frac{\partial \rho \mathbf{u}}{\partial t} + \nabla \cdot \rho \mathbf{u} \mathbf{u} = -\nabla p + \nabla \cdot \mu (\nabla \mathbf{u} + \nabla^T \mathbf{u}) + \int \sigma \kappa' \mathbf{n}' \delta^\beta(\mathbf{x} - \mathbf{x}') ds' + (\rho - \rho_f) \mathbf{g} + \mathbf{j} \times \mathbf{B}^0. \quad (2)$$

The pressure is denoted by p , μ is the dynamic viscosity, \mathbf{g} is the gravity vector, ρ_f is the density of the continuous phase, σ is the surface tension coefficient, k is the curvature, \mathbf{j} is the electric current and \mathbf{B}^0 is the applied magnetic field. The effect of the interface is accounted in the integral term that represents the surface tension force concentrated at the boundary of the two fluids. Since this force is calculated only at the interface this can be represented as two-dimensional delta function $\delta^\beta(\mathbf{x} - \mathbf{x}') = \delta(x - x')\delta(y - y')$, where \mathbf{x} is the point at which the equations are evaluated and \mathbf{x}' is a point in the interface. The equation for computing the induced magnetic field is given by:

$$0 = \eta \nabla^2 \mathbf{b} + (\mathbf{B}^0 \cdot \nabla) \mathbf{u} - (\mathbf{u} \cdot \nabla) \mathbf{B}^0, \quad (3)$$

where η is the magnetic diffusivity, \mathbf{b} and \mathbf{B}^0 are the induced and applied magnetic fields, respectively. Additionally, both the applied and induced magnetic field are solenoidal and satisfy:

$$\nabla \cdot \mathbf{b} = 0, \quad \nabla \cdot \mathbf{B}^0 = 0. \quad (4)$$

Once the induced magnetic field is calculated, the induced electric current can be found as:

$$\nabla \times \mathbf{b} = \mu_m \mathbf{j}^i, \quad (5)$$

where μ_m is the magnetic permeability. The set of Eqs. (1)-(5) were discretized using a mesh with 1024×2048 grid points that are uniformly spaced in the x - and y - directions and the finite volume method was implemented in an in-house code. A second order predictor-corrector method was implemented for the integration in time. We considered non-slip walls the top and bottom boundaries, and are separated 64 drop diameters apart. The lateral walls are also considered solid walls and are located 32 drop diameters away from each other, therefore, the computational domain is similar in size with respect to the experimental Hele Shaw cell. For solving the induction Eq. (3), the zero boundary conditions on \mathbf{b} are imposed at all the walls of the computational domain. The numerical simulations were carried out for similar conditions of the experimental observations. We must note that the applied magnetic field distribution is not constant, thus the motion of the conducting drop thorough the magnetic field will promote the existence of the induced magnetic field and consequently the induced currents according to Eqs. (3) and (5), respectively, which will generate a Lorentz force that will brake the motion of the metal drop.

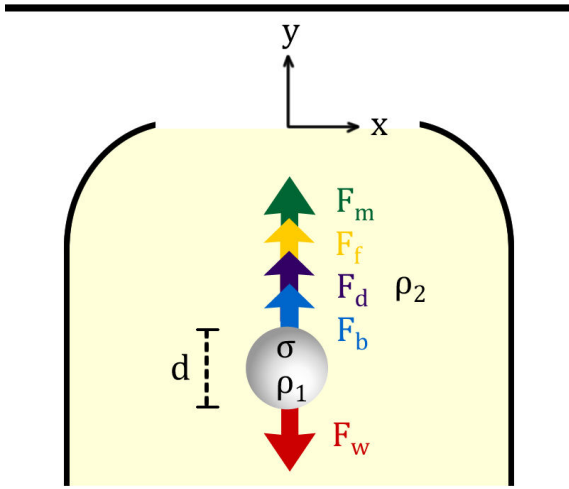


FIGURE 3. Force diagram on the liquid metal drop.

3.2. Analytical solution

Following the approach for the dynamics a spherical particle to a one-dimensional flow by Morsi [20], a simple approach of the drop dynamics is the balance of the forces (as seen in Fig. 3) which act on the liquid metal drop

$$F = F_d + F_b + F_m + F_f + F_w, \quad (6)$$

where F_d is the drag, F_b is the buoyancy, F_m is the induced magnetic force, F_f is the friction due to the walls of the cell and F_w is the weight. The latter forces can be mathematically expressed as

$$m \frac{dv}{dt} = \frac{1}{2} C_D \rho_2 A v^2 + \rho_2 V g + \sigma v B_z^0{}^2 + kv - \rho_1 V g, \quad (7)$$

where m is the mass of the metal drop, v is the velocity, t denotes time, C_D is the drag coefficient, A is the superficial area of the drop, V is the volume and g is the gravity acceleration, σ is the electrical conductivity, B_0 is the magnetic field intensity, ρ_1 and ρ_2 is the metal drop and the medium density, respectively, and k is a friction coefficient.

The total magnetic force (or Lorentz force) in the drop due to the induced currents is $\vec{F}_m = \int (\vec{j}^i \times \vec{B}^0) dV$. From the MHD point of view, the induced electric currents can be obtained through two different formulations, namely, the φ -formulation and the B -formulation. The first one departs from the Ohm's law, that is

$$\vec{j}^i = \sigma(\vec{E} + \vec{u} \times \vec{B}^0). \quad (8)$$

Considering that only the component of the applied magnetic field normal to the plane of motion is relevant, B_z^0 , and the drop moves in the negative y -direction, $-v$, the internal velocity is the one of the drop as it moves as a non-deformable solid. Since we know that the induced currents are generated in response to fluid motion in the applied magnetic field and not due to electric fields. Thus the main component of the induced current is $j_x^i = -\sigma v B_z^0$. The cross

product of the electric density current and the applied magnetic field ($\vec{j}^i \times \vec{B}^0$) is $\sigma v B_z^0{}^2$. Finally, the magnetic force is $\sigma v B_z^0{}^2 V$. The second formulation departs from the induction Eq. (3), which for the $x - y$ plane it reads

$$0 = \frac{1}{\mu_0 \sigma} \left(\frac{\partial^2 b_z}{\partial x^2} + \frac{\partial^2 b_z}{\partial y^2} \right) - u \frac{\partial B_z^0}{\partial x} - v \frac{\partial B_z^0}{\partial y}, \quad (9)$$

considering that the drop only moves in the negative y -direction and the induced magnetic field only depends the vertical direction, it goes as

$$\frac{1}{\mu_0 \sigma} \frac{\partial^2 b_z}{\partial y^2} = v \frac{\partial B_z^0}{\partial y}. \quad (10)$$

By integration by parts and assuming low acceleration ($v' < 1$) and the drop moves in the negative y -direction

$$\frac{\partial b_z}{\partial y} \approx -\mu_0 \sigma v B_z^0, \quad (11)$$

From Ampère's law (Eq. (5))

$$j_x^i = \frac{1}{\mu_0} \frac{\partial b_z}{\partial y} = -\sigma v B_z^0. \quad (12)$$

Consequently, the magnetic force ($\vec{j}^i \times \vec{B}^0$) in the positive y -direction is $\sigma v B_z^0{}^2$, which is the same result as the φ -formulation. As seen in Eq. (10), there should be a gradient of the applied magnetic field in order that the magnetic braking force exist. Rearranging Eq. (7) with $m = \rho_1 V$, and defining $\rho_r = \rho_2 / \rho_1$ we get

$$\frac{dv}{dt} = \frac{3C_D \rho_r}{d} v^2 + \left(\frac{\sigma B_z^0{}^2}{\rho_1} + \frac{k}{\rho_1} \right) v + g(\rho_r - 1), \quad (13)$$

where d is the diameter of the drop. By scaling the velocity and time with v_0 and d/v_0 , respectively, where v_0 is a characteristic velocity, the dimensionless equation for the velocity of the falling drop reads

$$\frac{dv}{dt} = 3C_D \rho_r v^2 + \left(\frac{Ha^2}{Re} + K \right) v + G(\rho_r - 1), \quad (14)$$

where the dimensionless parameters Re , Ha , K and G denotes the Reynolds number, Hartmann number and the dimensionless friction and gravity acceleration, respectively, which are defined as

$$Re = \frac{v_0 d}{\nu}, \quad Ha = dB_z^0 \sqrt{\frac{\sigma}{\rho_1 \nu}},$$

$$K = \frac{kd}{\rho_1 v_0}, \quad G = \frac{gd}{v_0^2}, \quad (15)$$

where ν is the kinematic viscosity. We note that, the behavior of MHD flows can be characterized by the Hartmann number, that represent a relation between magnetic with respect the viscous forces. The solution to the Eq. (14) is

$$v(t) = \frac{b - \sqrt{b^2 + 4ac}}{2a} \tanh \left(\frac{\sqrt{b^2 + 4ac}}{2} t \right), \quad (16)$$

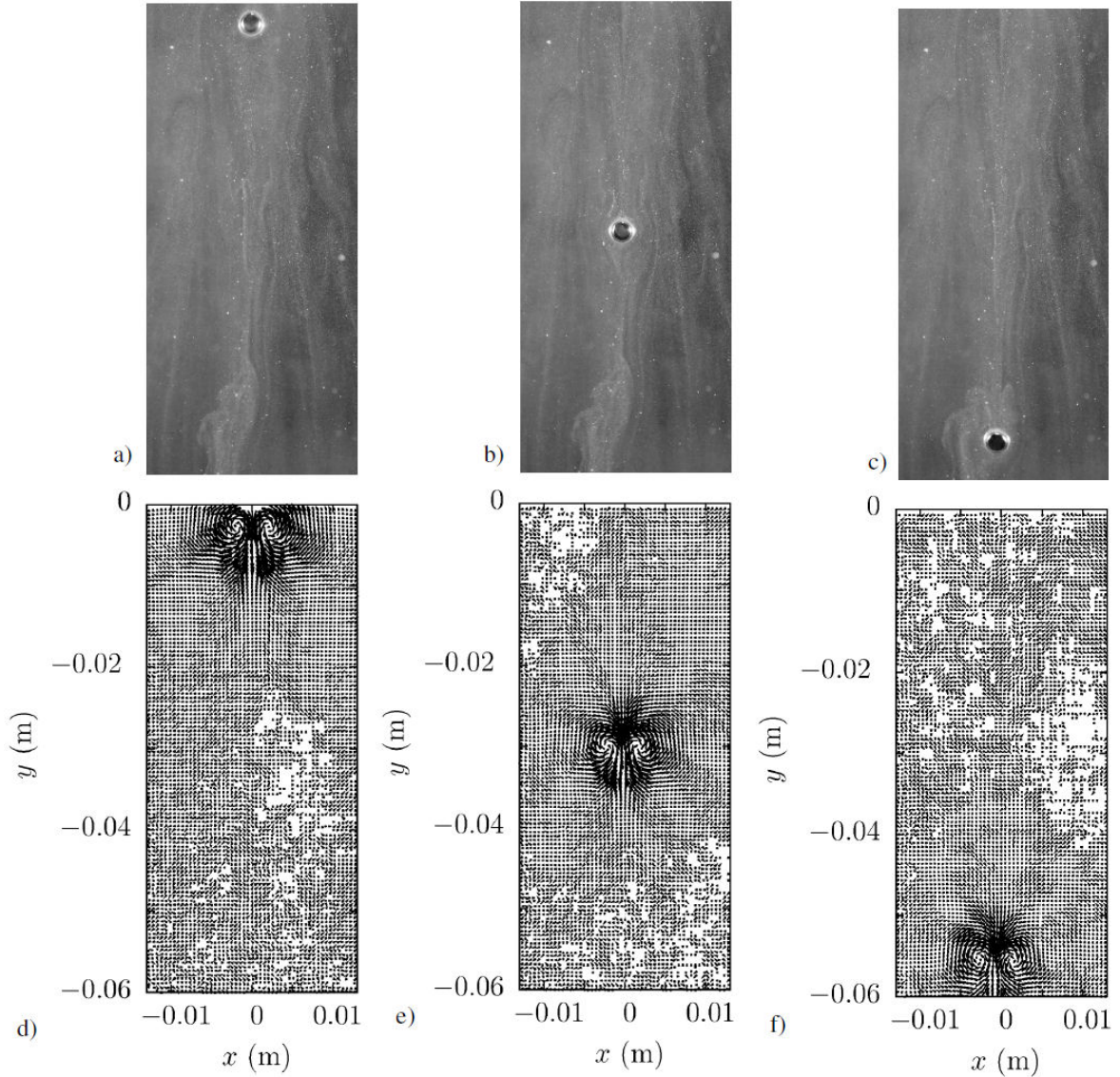


FIGURE 4. First row: Snapshots of the falling metal drop for $Ha = 0$ at different time instants $t = 0.5$ s, $t = 3.5$ s and $t = 6.8$ s. b) Second row: PIV velocity fields of the drop for the latter time instants. Experimental observations.

where the initial condition is zero. The parameters a , b and c are defined as

$$a = 3C_D\rho_r, \quad b = \frac{Ha^2}{Re} + K, \quad c = G(\rho_r - 1). \quad (17)$$

The drag coefficient C_D can be obtained from [20]

$$C_D = \frac{k_1}{Re} + \frac{k_2}{Re^2} + k_3. \quad (18)$$

Finally, if the solution for the velocity (Eq. (16)) is integrated, we can obtain the position of the drop as a function of time

$$y(t) = \frac{\log(\cosh[\frac{1}{2}\sqrt{b^2+4ac}t]) (2b-2\sqrt{b^2+4ac})}{2a\sqrt{b^2+4ac}}. \quad (19)$$

We must note that, this is an idealized model that can

only be compared with the experiments in a qualitative level as will be shown in next section.

4. Results

Figure 4 show the experimental snapshots of the falling metal drop (first row) along with the vector fields (second row) for different time instants. The vector fields allows to easily identify the flow structure as the metal drop falls surrounded with the glycerin, namely, a dipole vortex. Moreover, the vector fields allow us also to identify the direction of the flow and its magnitude.

The tracking of the metal drop allows to obtain the position of the drop in every frame of the recorded video, Fig. 5 shows the position of the drop as a function of time. We can

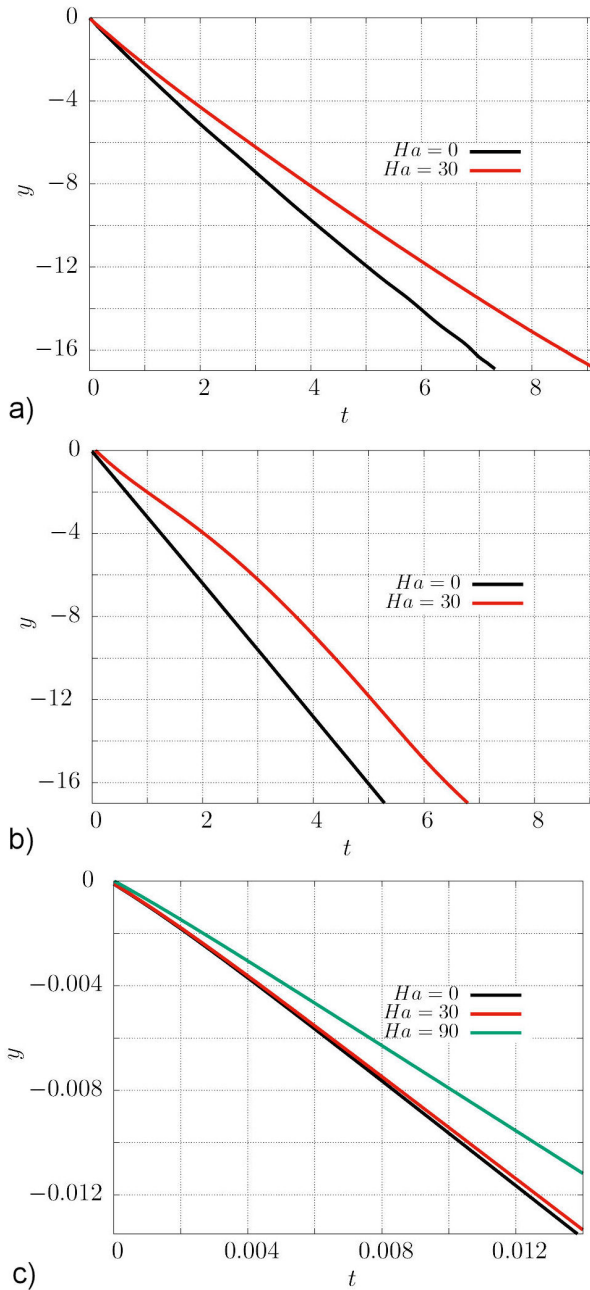


FIGURE 5. Vertical position y of the metal drop as a function of time t . a) Experimental data. b) Numerical simulation. c) Analytical solution from Eq. (19).

observe that for the hydrodynamics case, that is $Ha = 0$, the drop traverses the domain presented in Fig. 5a) ($l = 0.06$ m) in $t = 7.3$ s, meanwhile it lasts $t = 9.1$ s when the induced magnetic effects are present, in this case the Hartmann number is $Ha = 30$. The above shows the braking effect on the drop due to the presence of the magnetic field gradient. Because the relative motion of the droplet with respect to the magnetic field, induced currents are generated. The interaction of the induced currents and the applied magnetic field produce a Lorentz force in the metal drop. This electromagnetic force is produced in the opposite direction of accelera-

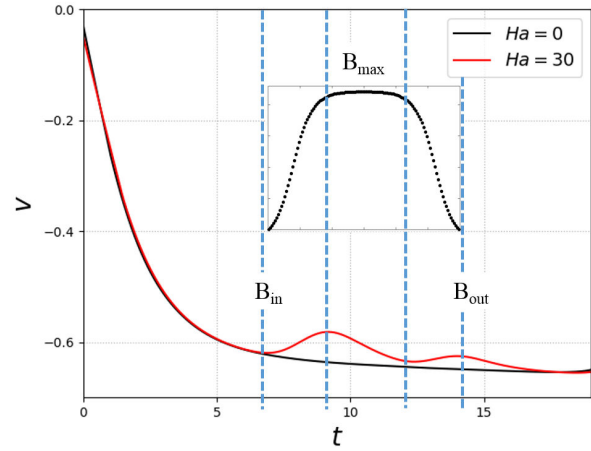


FIGURE 6. Velocity of the drop v as a function of time t . Numerical simulation.

tion of gravity and as a consequence slows down the motion of the drop. From the latter data, we can calculate a mean velocity: $v_m = -7.7 \times 10^{-3}$ m/s and $v_m = -6.2 \times 10^{-3}$ m/s, for $Ha = 0$ is and $Ha = 30$, respectively.

The Reynolds number for the experiments is $Re = v_m d / \nu = 76$, which demonstrates that the flow regime is laminar and can be compared with the theoretical models. Correspondingly, the position of the drop as a function of time from the numerical simulations for $Ha = 0$ and $H = 30$ is shown in Fig. 5b). The braking of the metal drop when the induced effects are present is also observed and the agreement with the experimental results is quantitative. Concerning the analytical solution, Fig. 5c) shows the position of the drop from calculated form Eq. (19). Taking the characteristic velocity is the mean velocity of the experimental falling drop in the hydrodynamics case, $v_0 = v_m$ and the friction factor is $k = 0.143$ Kg/s, we obtain $G = 555$ and $K = 442$. The coefficients for the drag coefficient are $k_1 = 46.5$, $k_2 = -116.67$ and $k_3 = 0.6167$, since $10 < Re < 100$. As it is shown, the theoretical results are qualitatively consistent to that found experimentally (Fig. 5a)). The braking effect promoted by the Lorentz force on the drop is clearly observed for the case of $Ha = 30$ with respect to the purely hydrodynamic flow ($Ha = 0$), and as the Hartmann number is increased the braking is larger ($Ha = 90$).

Simulations are able to give a deep insight in the drop motion and flow generated function of time. In Fig. 6, the velocity of the metal drop as function of time is presented computed from the numerical simulations. The vertical lines mark the instants of time in which the metal drop enters and leaves the magnetic field. Additionally, the instant where the drop is in the area where the field produced by the magnet permanently is maximum is also marked. As it can be observed, once the metal drop enters in the magnetic field, the extra drag promoted by the Lorentz force causes a deceleration of the drop, in this zone a high magnetic field gradient promotes that the Lorentz force be intense. Once the drop leaves the magnetic field, it accelerates until reaches the ap-

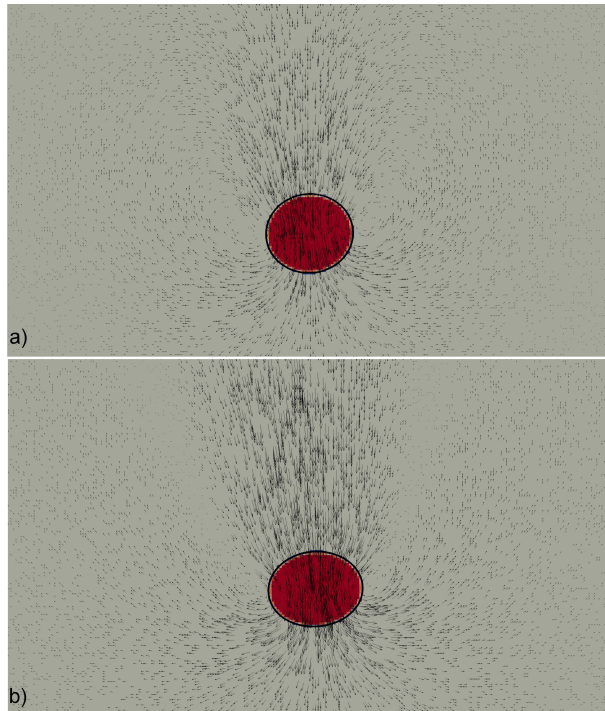


FIGURE 7. Velocity field (black arrows) and falling metal drop (red color). a) $Ha = 0$. b) $Ha = 30$. Numerical simulations.

proximately the same velocity of the $Ha = 0$ case. The interaction found is consistent with the analytical and numerical results reported by [11, 13], respectively, but in this case, the effect of the Lorentz force on the metal drop dynamics is shown for a case that can be reproduced by an experiment using an approximation of a real magnetic field distribution generated for a given permanent magnet.

Figure 7, the falling metal drop and the velocity field are shown at the same instant of time for $Ha = 0$ and $Ha = 30$. For both cases the flow formed around the drop is a dipole vortex, as seen in the experimental PIV results (second row in Fig. 4). Due to the low Reynolds number, for both simulations, the metal drop follows an approximately straight path along its fall, which matches with the one-dimensional flow assumption in the analytic solution. In the case of $Ha = 0$, the drop tends to remain with a circular shape during all the trajectory, while for $Ha = 30$, the drop shape changes to an ellipse due to the Lorentz force promoted by the interaction of the induced current and the applied magnetic field. As it was commented, the Lorentz force acts in the opposite direction of the gravity acceleration in the zones where the applied magnetic field gradient is intense, and this force acts as a brake on the motion of the drop.

In order to explain how the Lorentz force produces a braking effect on the drop's motion, the electric current density vector and contours of the induced magnetic fields inside the metal drop are shown in Fig. 8. The induced current mainly points in the negative x -direction, while the magnetic field is in the z -direction, thus the magnetic force is in the y -direction which is contrary to the drop's motion. As can be appreciated, due to the deformation and the internal flow inside the

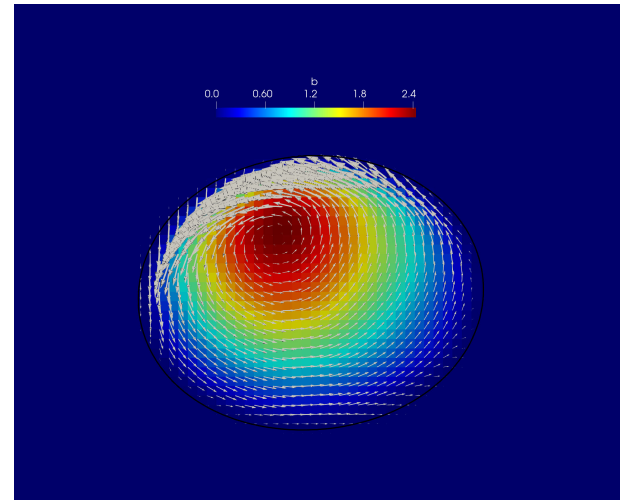


FIGURE 8. Induced magnetic field contour plot and induced current density vector field inside the falling metal drop, $Ha = 30$. Numerical simulations.

drop, the electric currents form non-axisymmetric closed loops along polar axis. The small deviation from a rectilinear path due to the Reynolds number reached by the drop promotes that it does not pass through out the central line of the permanent magnet making the electric currents and induced magnetic field not symmetric with respect to the longitudinal axis of the metal drop. The symmetric case for the induced currents occurs the drop is a non-deformable solid [11].

5. Concluding remarks

The falling metal drop falling in a localized magnetic field has been studied theoretically and experimentally in the laminar regime ($Re = 76$). The metal drop falling in glycerin was observed experimentally through PIV and image tracking. An analytical solution for the falling drop under several body forces was derived. A numerical solution based on the so-called front-tracking method for the incompressible Navier-Stokes equations was implemented. The simulations were performed for a size similar to the experimental Hele-Shaw cell in order to analyze the complete trajectory of the metal drop, including the zone where it interacts with the applied magnetic field. It was found that at the zones in which is a intense magnetic field gradient, the drop decelerates due to the generated Lorentz force that counteracts the gravity acceleration, however, in the zone where the applied magnetic field is approximately constant, there is no electromagnetic interaction between the metal drop and the permanent magnet. The flow and electrical current were also analyzed and it was found that at the presented flow conditions, the Lorentz force tends to deform the drop, also, the unbalance in the pressure gradient promoted by the reached Reynolds number deviates the drop from a rectilinear path and as a consequence, the induced currents and magnetic field inside the drop are non symmetric with respect to the longitudinal axis of the metal drop. The analytical and numerical solutions

represent qualitatively the experimental problem. To the best of our knowledge, this is the first reported experimental study for liquid metal drops falling in the presence of a perpendicular non-uniform magnetic field.

Acknowledgements

This research was supported by CONACYT, Mexico, under project 258623. A.F. and S.P. thank the Cátedras program from CONACYT. Material support from Sergio Cuevas (IER-UNAM) is also thanked.

1. P. A. Davidson, *Introduction to Magnetohydrodynamics*, (Cambridge University Press 2017).
2. L. Bühler, C. Mistrangelo and H. J. Brinkmann *Experimental investigation of liquid metal MHD flow entering a flow channel insert*. Fusion Engineering and Design, **154** (2020) 111484, <https://doi.org/10.1016/j.fusengdes.2020.111484>
3. Z. H. Wang and T. Y. Lei, *Liquid metal MHD effect and heat transfer research in a rectangular duct with micro-channels under a magnetic field*. International Journal of Thermal Sciences, **155** (2020) 106411, <https://doi.org/10.1016/j.ijthermalsci.2020.106411>
4. L. Bühler, J. Brinkmann and C. Koehly, *Experimental study of liquid metal magnetohydrodynamic flows near gaps between flow channel inserts*. Fusion Engineering and Design, **146** (2019) 1399, <https://doi.org/10.1016/j.fusengdes.2018.11.034>
5. Y. Mori, K. Hijikata, and I. Kuriyama, *Experimental Study of Bubble Motion in Mercury With and Without a Magnetic Field*. Journal of Heat Transfer, **99** (1977) 404, <https://doi.org/10.1115/1.3450710>
6. T. Tagawa, *Numerical simulation of two-phase flows in the presence of a magnetic field*. Mathematics and Computers in Simulation, **72** (2006) 212, <https://doi.org/10.1016/j.matcom.2006.05.040>
7. J. Zhang, and M. J. Ni, *Direct simulation of single bubble motion under vertical magnetic field: Paths and wakes*. Physics of Fluids, **26** (2014) 102102, <https://doi.org/10.1063/1.4896775>
8. P. Nikos, B. Lefteris, and G. Rui, *Deflection of a liquid metal jet/drop in a tokamak environment*, Fusion Engineering and Design, **89** (2014) 2930, <https://doi.org/10.1016/j.fusengdes.2014.09.004>.
9. T. Wanga, T. Kwokb, C. Zhoua and S. Vaderc, *In-situ droplet inspection and closed-loop control system using machine learning for liquid metal jet printing*. Journal of Manufacturing Systems, **47** (2018) 83, <https://doi.org/10.1016/j.jmsy.2018.04.003>.
10. D. Ehrenreich *et al.*, *Nightside condensation of iron in an ultrahot giant exoplanet*. Nature, **580** (2020) 597, <https://doi.org/10.1038/s41586-020-2107-1>
11. J. Walker and W.M. Wells, *Drag force on a conductive spherical drop in a nonuniform magnetic field*. ORNL/TM-6976 (Sept. 1979).
12. T. Tagawa, *Numerical Simulation of a Falling Droplet of Liquid Metal into a Liquid Layer in the Presence of a Uniform Vertical Magnetic Field*. ISIJ International, **45** (2005) 954, <https://doi.org/10.2355/isijinternational.45.954>
13. S. Wu, J. Zhang and M.J. Ni, *Numerical study of a single droplet falling through a nonuniform horizontal magnetic field with a constant gradient*. Int. J. Multiph. Flow, **110** (2019) 18, <https://doi.org/10.1016/j.ijmultiphaseflow.2018.08.006>
14. B. Gol, M.E. Kurdzinski, F.J. Tovar-Lopez, P. Petersen, A. Mitchell and K. Khoshmanesh *Hydrodynamic directional control of liquid metal droplets within a microfluidic flow focusing system*. Appl. Phys. Lett, **108** (2016) 164101, <https://doi.org/10.1063/1.4947272>
15. W. Thielicke and E.-J. Stamhuis, *PIVlab - Time-Resolved Digital Particle Image Velocimetry Tool for MATLAB*, Version 1.41. (2014), <http://dx.doi.org/10.6084/m9.figshare.1092508>
16. A. Figueroa, F. Demiaux, S. Cuevas and E. Ramos, *Electrically driven vortices in a weak dipolar magnetic field in a shallow electrolytic layer*. J. Fluid Mech. **641** (2009) 245, <https://doi.org/10.1017/S0022112009991868>
17. G. Tryggvason, R. Scardovelli, S. Zaleski, *Direct numerical simulations of gas-liquid multiphase flows*, Cambridge Press, 1st edn., 2011.
18. S. Piedra, E. Ramos and J.-R. Herrera, *Dynamics of two-dimensional bubbles*. Phys. Rev. E., **91** (2015) 063013, <https://doi.org/10.1103/PhysRevE.91.063013>
19. Moreau R. (1990) *Magnetohydrodynamics*, Kluwer.
20. S. A. Morsi and A. J. Alexander, *An investigation of particle trajectories in two-phase flow systems*. J. Fluid Mech., **55** (1971) 193, <https://doi.org/10.1017/S0022112072001806>